Received: 27 January 2024 | Revised: 23 March 2024 | Accepted: 24 March 2024

DOI: 10.1002/pc.28404

RESEARCH ARTICLE

Polymer COMPOSITES WILEY

Enhancing flame retardancy, anti-impact, and corrosive resistance of TPU nanocomposites using surface decoration of α-ZrP

Sensen Han[1] | **Shuangshan Li**[1] | **Dongyan Liu**[2] | **Yu Dong**[3] | **Ziqi Gao**[1] | **Yanxi Zhang**[4] | **Qingshi Meng**[1]

[1]College of Aerospace Engineering, Shenyang Aerospace University, Shenyang, China

[2]Shi-changxu Innovation Center for Advanced Materials, Institute of Metal Research, Chinese Academy of Sciences, Shenyang, China

[3]School of Civil and Mechanical Engineering, Curtin University, Perth, Western Australia, Australia

[4]School of International Education, Shenyang Aerospace University, Shenyang, China

Correspondence

Yu Dong, School of Civil and Mechanical Engineering, Curtin University, GPO Box U1987, Perth, WA 6845, Australia.
Email: y.dong@curtin.edu.au

Qingshi Meng, College of Aerospace Engineering, Shenyang Aerospace University, Shenyang 110136, China.
Email: mengqingshi@sau.edu.cn

Funding information

Liaoning Provincial Department of Education Series Project, China, Grant/Award Number: LJKZ0187; National Natural Science Foundation of China, Grant/Award Number: 52173077; Liaoning BaiQianWan Talents Program, Grant/Award Number: 2021921081; Natural Science Foundation of Liaoning Province, Grant/Award Number: 2023-MS-239

Abstract

The development of polyurethane composites with significant flame retardancy and corrosion resistance for widening its practical application is a great importance. In this study, supramolecular wrapped α-ZrP (MCP@ZrP) was prepared via self-assembly of melamine, cobalt ions (Co^{2+}) and phytic acid (PA) on the surfaces of α-zirconium phosphate (α-ZrP). It was found that both compatibility and dispersion of α-ZrP sheets in thermoplastic polyurethane (TPU) matrices were improved with the incorporation of organic supramolecular components in TPU/MCP@ZrP nanocomposites. Moreover, their fire-retardant characteristic was significantly enhanced, along with effective suppression of smoke and toxic gas emission. By adding 5 wt% MCP@ZrP, peak heat release rate, total heat release, total smoke production, and total CO production of such nanocomposites were reduced by 35.66%, 18.01%, 15.52%, and 41.42%, respectively. The generation of a continuous and dense char layer benefited from well-dispersed MCP@ZrP nanohybrids, which resulted in tortuous effect to impede heat diffusion and prevent the evaporation of volatile gasses. By means of the barrier effect of ZrP, TPU/MCP@ZrP composite films also showed improved anticorrosion performance. Effective interfacial adhesion, achieved by combining MCP supermolecules and α-ZrP sheets, offers a viable approach to improve protective properties of TPU nanocomposites.

Highlights

- Supramolecular-wrapped α-ZrP was prepared via self-assembly strategy.
- MCP@ZrP showed good dispersion and interface adhesion within TPU matrices.
- MCP@ZrP enhanced the flame retardancy and mechanical performance of TPU.
- MCP@ZrP preventing smoke and toxic gas evaporation.

KEYWORDS
anti-impact, corrosion resistance, fire retardancy, thermoplastic polyurethane (TPU)

1 | INTRODUCTION

Thermoplastic polyurethane (TPU) as a versatile elastomer has been widely used in automotive, industrial, and aerospace owing to its exceptional abrasion resistance, flexibility, hydrolytic resistance, as well as hardness.[1–3] Unfortunately, TPU, which is similar to many other polymeric materials, is prone to high flammability along with the emission of great quantities of soot and toxic gasses in the combustion process,[4,5] thus leading to irreparably detrimental environmental pollution. As such, it is necessary to develop a novel, highly efficient and environmentally friendly flame retardant to mitigate fire hazards and emission of toxic gasses in relation to TPU products.

In recent decades, various nanomaterials have been developed as flame retardants for polymer,[6–10] as evidenced by MXene,[11] boron nitride,[12,13] black phosphorous,[14] halloysite nanotubes (HNTs),[15] and graphene.[16] To meet the growing demand for fire retardance, it is essential to focus on new functional nanofillers. Recently, α-zirconium phosphate (α-ZrP) has drawn significant attention because of its unique characteristics including ion-exchange, thermal and chemical stabilities, catalytic activity, as well as intercalation in polymers. As a solid acid catalyst, α-ZrP nanosheets can enhance the carbonization degree of char residues and hinder toxic gas and heat transfer due to their well-organized lamellar structures. Consequently, they are often applied as functional additives in polymer matrices to improve flame retardancy.[17–19] Nevertheless, the solid acid sites in α-ZrP can compromise flame retardancy by accelerating early-stage degradation. Overall, it is vital to shield these solid acid sites from intimate contacts with polymeric chains during the whole process. In addition, the aggregation of α-ZrP nanosheets and their adhesion with the polymer matrix are also the problems to solve when they are incorporated into polymers. As reviewed, nanomaterials modified by supramolecular aggregates in conjunction with flame retardants have been in rapid progress in the last few decades.[20–22] Hydrogen bonding self-assembly and other interactions offer unique structural properties with a great potential for use in preparing flame retardants based on polymers. Wang et al.[12] fabricated multifunctional BN nanosheets by enclosing phytic acid doped polypyrrole shell, followed by adsorbing copper ions to acquire flame-retardant additives into TPU. Shi et al.[11] prepared a multifunctional nanohybrided flame retardant of $Ti_3C_2T_x$@MCA for TPU by engineering $Ti_3C_2T_x$ surfaces with melamine cyanurate (MCA) via supramolecular assembly. By virtue of the supramolecular self-assembly, Cheng et al. reported a novel and extremely efficacious an in-situ manufacturing strategy to prepare melamine/phytic acid (PAMA)/Si_3N_4 (SW-Si_3N_4) hybrid sandwich sheets. Xie et al.[23,24] constructed an organic–inorganic nanohybrid network in polymers, which induces an attractive hybrid strategy to improve the toughness, strength, and flame retardancy of polymers.

As inspired by the self-assembly mechanism,[23,25] ionic bonding and electrostatic interaction between melamine and phytic acid (PA) bridged with cobalt ions (Co^{2+}) rapidly form the ternary hybrid of MCP supramolecular aggregates with high ionic cross-linking density. MCP supramolecule offers efficient catalytic activities and enhances integrated properties along with the contribution of P and N atoms for flame retardancy in the particular process of polymer combustion. It could be hypothesized that MCP supramolecular aggregates supported on α-ZrP nanosheet surfaces enabled to improve fire retardancy and suppress toxic gas release of TPU. In this study, we reported a green fabrication strategy to exfoliate α-ZrP nanosheets via glucose-assisted ball milling. Then supramolecular aggregates are comprised of melamine/Co^{2+}/phytic-acid self-assembled on α-ZrP nanosheet surfaces to generate a nanohybrid flame retardant (MCP@ZrP). The electrostatic self-assembly of MCP supermolecules onto α-ZrP nanosheets facilitates uniform dispersion and improves interfacial adhesion within TPU matrices. MCP@ZrP nanohybrids combine the merits of α-ZrP nanosheets and MCP supermolecules, which can function as an extremely efficacious flame retardant. MCP@ZrP nanohybrids were then incorporated into TPU matrices for the investigation of their fire retardancy, anti-impact, and corrosion resistance performance. It is anticipated in this study that the hybridization of α-ZrP nanosheets and MCP supermolecules could effectively improve flame retardancy and retard the emission of toxic gasses in TPU nanocomposites. Additionally, corrosive resistance of TPU films is anticipated to be improved by incorporating well-dispersed α-ZrP nanosheets.

2 | EXPERIMENT DETAILS

2.1 | Materials

Thermoplastic polyurethane (polyether-based TPU, 1180A) was obtained from BASF Polyurethane Specialties

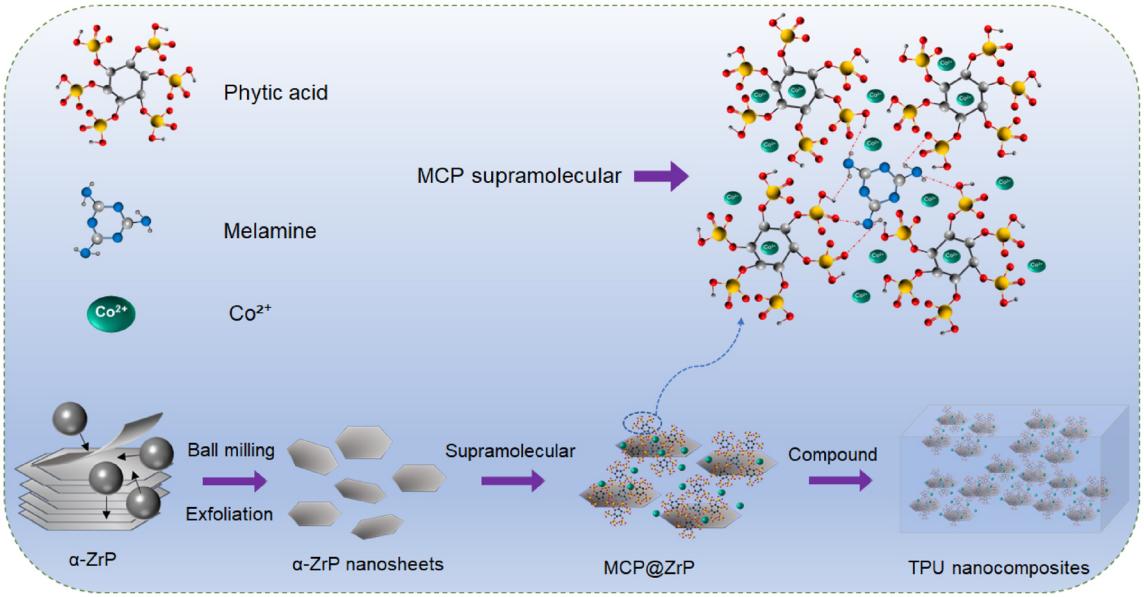

FIGURE 1 Schematic diagram of the detailed preparation of TPU/MCP@ZrP nanocomposites.

Co., Ltd. (Shanghai, China). α-ZrP was provided by Sunshine Factory Co., Ltd. (Mianzhu, Sichuan, China). A 70% phytic acid (PA) solution, melamine and cobalt nitrate hexahydrate ($Co(NO_3)_2{\cdot}6H_2O$) were supplied by Aladdin Biochemical Technology Co., Ltd. (Shanghai, China). All chemicals were used as received without further purification.

2.2 | Preparation of samples

2.2.1 | Preparation of α-ZrP nanosheets

In a typical process, pristine α-ZrP (3.0 g, average size = 325 mesh, 99.5%), 75 wt% glucose syrup (50 mL), as well as two different sizes of ZrO_2 balls with diameters of 8 mm (80 g) and 2 mm (40 g) were loaded into a 250 mL ZrO_2 jar. The jar was rotated in a planetary ball mill (F-P4000E, Hunan Focucy Experimental Instrument Co., Ltd., China) at 400 rpm for 10 h under a cooling system. Finally, ball-milling exfoliated α-ZrP nanosheets were prepared by the multisteps of centrifugation, washing, and freeze-drying.

2.2.2 | Preparation of MCP@ZrP nanohybrids

A 0.2 g exfoliated α-ZrP nanosheets were dispersed in 200 mL deionized water for 4 h to create a uniform suspension. Subsequently, 0.2 g melamine and 2 mL PA solution were added into the suspension under magnetic stirring for 3 h at 95°C. Further, 0.1 g $Co(NO_3)_2{\cdot}6H_2O$ was slowly added into the above-mentioned suspension. The adsorption of Co^{2+} was carried out for additional 2 h under continuous magnetic stirring. The temperature was kept at 95°C. The final product of MCP@ZrP was then obtained by the centrifugation, and further washed with deionized water, methanol, and ethanol several times prior to freeze-drying.

2.2.3 | Preparation of TPU/MCP@ZrP nanocomposites

TPU nanocomposites were fabricated by a co-coagulation and hot press, as shown in Figure 1. Typically, the preparation of TPU nanocomposites containing 5.0 wt% MCP@ZrP is detailed in the following. A 2.5 g MCP@ZrP nanohybrid was dispersed in 300 mL dimethylformamide (DMF) under sonication for 1 h. Subsequently, 47.5 g TPU was added into uniform dispersed mixture mentioned earlier and stirred until TPU was completely dissolved at 90°C. The uniformly dispersed mixture was poured into DI water prior to mechanical stirring. The flocculate was washed with DI water and absolute ethanol several times, and was then dried at 80°C for 12 h to remove residual solvents. Finally, the sample was hot pressed at 180°C and 10 MPa for 10 min with the standard size for further characterizations. Other TPU nanocomposites were fabricated using the similar procedure.

3 | RESULTS AND DISCUSSION

3.1 | MCP@ZrP nanohybrids

X-ray diffraction (XRD) patterns were applied to investigate crystal structures of α-ZrP and MCP@ZrP nanohybrids, as

illustrated in Figure 2A. As for α-ZrP, three typical diffraction peaks at $2\theta = 11.6°$, 19.7°, and 24.9° (JCPDS: 33–1482) were detected, corresponding to (002), (110), and (112) planes, respectively. In contrast, the intensity of (002) diffraction peak for α-ZrP in MCP@ZrP nanohybrids was reduced, which suggested that the decreased nanosheet stacking and an increased interlayer spacing with the presence of MCP supramolecules.

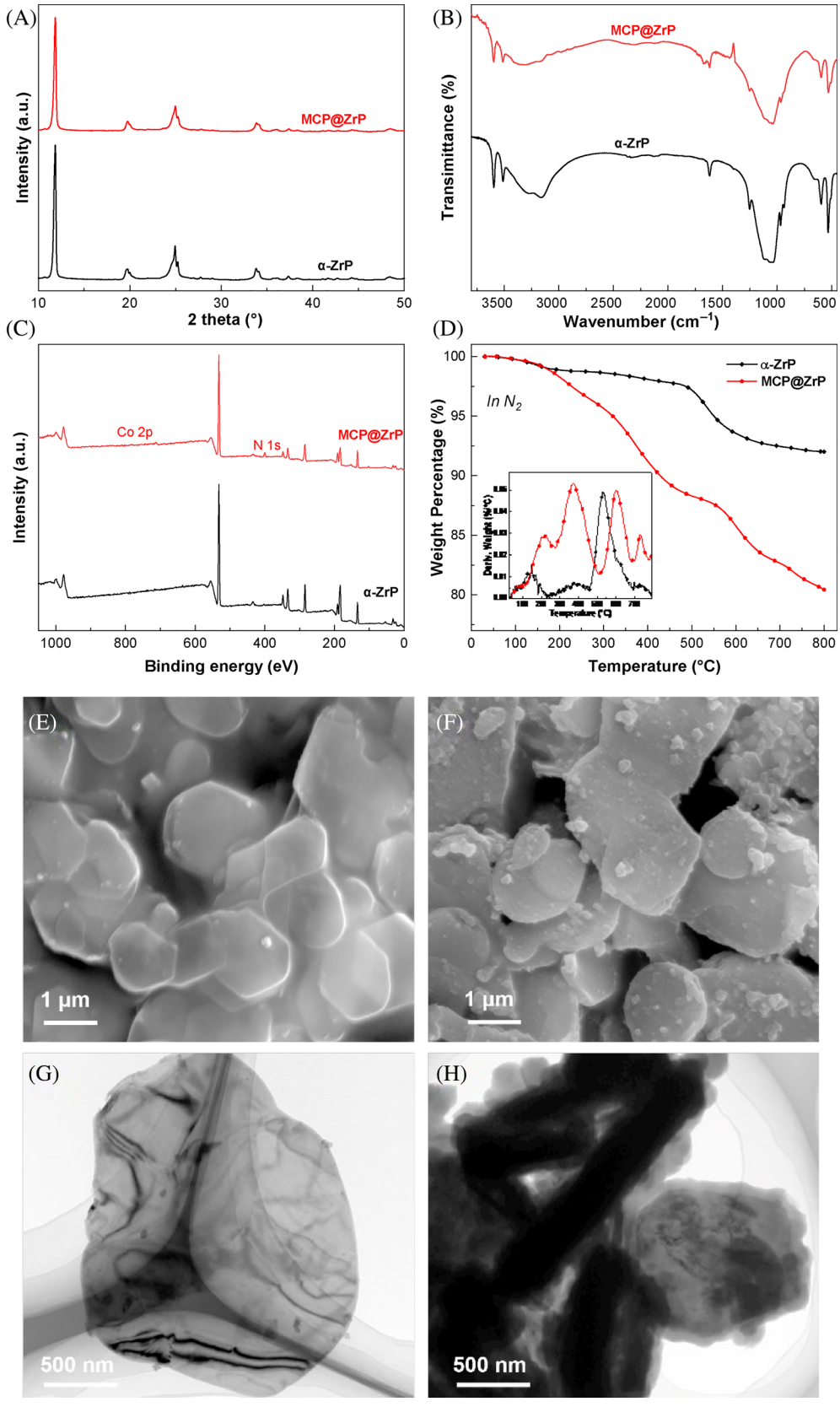

FIGURE 2 Microstructural characterization of α-ZrP and MCP@ZrP nanohybrids: (A) XRD, (B) FTIR, (C) TGA, (D) XPS, SEM for (E) α-ZrP and (F) MCP@ZrP, as well as TEM for (G) α-ZrP and (H) MCP@ZrP. FTIR, Fourier transform infrared Spectrometery; SEM, scanning electron microscopy; TEM, transmission electron microscopy; TGA, thermal gravimetric analysis; XPS, x-ray photoelectron spectroscopy; XRD, x-ray diffractometry.

The structural configuration of α-ZrP and MCP@ZrP nanohybrids was examined by Fourier transform infrared (FTIR) analysis, as evidenced in Figure 2B. The peaks identified at 3593 and 3510 cm^{-1} in the α-ZrP spectrum were assigned to asymmetric stretching vibrations of O—H groups inside α-ZrP layers.[18] The peaks observed at 1120 and 1050 cm^{-1} could be referred to as the symmetric and asymmetric stretchings of P—O bonds in PO_2 groups respectively while broad absorption bands took place in the wavenumber range of 1200–1000 cm^{-1}. The vibration peaks of Zr—O bonds were located at 543 and 629 cm^{-1} in α-ZrP spectrum. In the case of MCP@ZrP nanohybrids, two new peaks detected at 3396 and 3230 cm^{-1} were associated with symmetric and asymmetric vibrations of —NH groups with respect to melamine. On the other hand, the peak occurrence at 1662 cm^{-1} was associated with the stretching vibration of $—NH_2$. The presence of these new peaks further proved successful modification of nanosheets with MCP supramolecule.

To gain deeper understanding as to the chemical composition of α-ZrP and MCP@ZrP nanohybrids, x-ray photoelectron spectroscopy (XPS) results as illustrated in Figure 2C. The XPS spectrum of MCP@ZrP nanohybrids exhibited distinct Co 2p and N 1 s peaks, which appeared to be absent in the α-ZrP spectrum. This finding offers the strong evidence for successful modification of nanosheets with MCP supramolecule, which indicated the formation of new nanohybrids with the change of chemical properties.

The thermal properties of α-ZrP and MCP@ZrP nanohybrids were investigated by thermal gravimetric analysis (TGA) under N_2 atmosphere in Figure 2D. The dehydration of α-ZrP occurred in the temperature range of 140–200°C, which was attributed to the volatilization of water. Subsequently, a condensation reaction occurred between the monohydrogen phosphate (P—OH) groups, leading to the formation of zirconium pyrosphosphate (ZrP_2O_7) at approximately 580°C. In contrast, it was revealed that the thermal decomposition behavior of MCP@ZrP induced a noticeable weight decrease, corresponding to the pyrolysis of grafted MCP supramolecules. Furthermore, the char yields of α-ZrP and MCP@ZrP at 800°C were found to be 92.01 and 80.44 wt%, respectively. Such results suggested that approximately 11.57 wt% MCP supramolecules could be successfully incorporated onto α-ZrP surfaces.

Scanning electron microscopy (SEM) and transmission electron microscopy (TEM) analyses were utilized to investigate the morphology of α-ZrP and MCP@ZrP nanohybrids. The laminar and smooth α-ZrP nanosheets were clearly shown in Figure 2E,G. A typical translucent sheet morphology, as depicted in Figure 2G, implied that pristine α-ZrP particles possessed the potential to undergo substantial exfoliation into thin nanosheets through the process of ball milling. After the wrapping of MCP supermolecules, rough surfaces could be observed for MCP@ZrP nanohybrids in Figure 2F,H. The morphology analysis of MCP@ZrP nanohybrids was consistent with associated results obtained via XRD, FTIR, XPS, and TGA. As a whole, MCP supermolecules were proven to be successfully integrated into α-ZrP nanosheet surfaces.

3.2 | Fracture morphology

Cryogenically fracture surfaces of TPU nanocomposites were observed via SEM analysis in order to visually evaluate interfacial adhesion between TPU matrices and nanoadditives. Overall, there appeared to be a smooth cross-section detected in neat TPU shown in Figure 3A1. However, when randomly selected area was magnified according to Figure 3A2, wave-like fracture surfaces

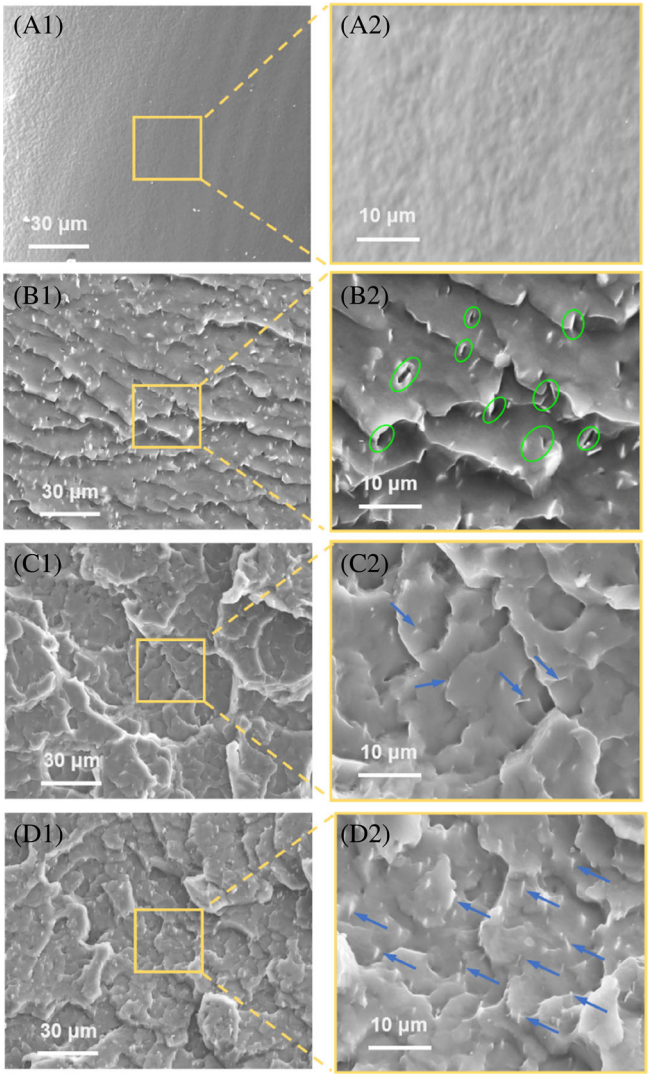

FIGURE 3 Scanning electron microscopy images for fractured surfaces: (A) neat thermoplastic polyurethane (TPU), (B) TPU/ZrP-2% nanocomposites, (C) TPU/MCP@ZrP-2% nanocomposites, and (D) TPU/MCP@ZrP-5% nanocomposites.

became manifested, which suggested better fracture resistance of TPU at low temperatures.

Unlike neat TPU, TPU nanocomposites reinforced with 2 wt% α-ZrP yielded coarse-grained fracture morphology, as illustrated in Figure 3B1. Nonetheless, there appeared to be a phase-separation phenomenon of α-ZrP nanosheets within TPU matrices, thus leading to a large number of cracks at the interfaces in Figure 3B2 and poor compatibility between α-ZrP nanosheets and TPU matrices. With the functionalization of MCP supermolecules, MCP@ZrP nanohybrids could interact better with TPU molecular chains without any slits according to Figure 3C1. As such, it was quite convincing that MCP@ZrP nanohybrids enabled to be uniformly dispersed into TPU matrices. When considering Figure 3C2 at the higher magnification. A typical suppression of phase separation was evident for aforementioned phase separation. When the addition of MCP@ZrP nanohybrids increased up to 5 wt%, the fracture surfaces became much rougher exhibited in Figure 3D1, which implied that the incorporation of MCP@ZrP nanohybrids tended to dissipate more energy during the fracture. In particular, at the high magnification in Figure 3D2, phase separation disappeared with a clear sign of typically good compatibility between MCP@ZrP and TPU matrices.

To investigate the elemental distribution in fractured surfaces of TPU/MCP@ZrP-5% nanocomposites, energy-dispersive X-ray spectroscopy mapping was carried out, and the results were shown in Figure S1. The characteristic elements of MCP, namely nitrogen (N) and cobalt (Co), were detected along with zirconium (Zr) in relation to α-ZrP. The relatively uniformly distribution of these elements (i.e., N, P, Co, and Zr) confirmed the homogeneous MCP@ZrP nanohybrids existing in TPU matrices.

TEM analysis is widely used to investigate the morphology of nanoadditives and their dispersion state in TPU matrices. Figure 4A presents a low-magnification micrograph of TPU/ZrP-2% where α-ZrP sheets tended to aggregate due to the occurrence of microsized clusters of α-ZrP sheets in TPU matrices. Under a close examination, it was revealed that the aggregation of α-ZrP sheets took place in Figure 4B, which could be ascribed to great van der Waals forces between the sheets owing to their large specific surface areas on the nanoscale. Such clusters were believed to deteriorate the reinforcing effectiveness of α-ZrP sheets within TPU matrices. With the modification of α-ZrP sheets using MCP, nanohybrids were separated and exfoliated, thus enabling to be homogeneously dispersed within the matrices. As illustrated in Figure 4C, MCP@ZrP nanohybrids tended to be a gray phase while huge clusters depicted in Figure 4B no longer existed in the matrices. Additionally, it was worth noting from Figure 4D that MCP@ZrP was proven to be firmly embedded within matrices. XRD was conducted to determine crystallographic structures of neat TPU and its corresponding nanocomposites according to Figure 4E. The XRD curve of neat TPU exhibited a broad peak located at $2\theta = 20.8°$, corresponding to the typical crystallization of hard segments in TPU molecules.[26] The XRD results also suggested the existence of intercalated and/or exfoliated microstructures in TPU nanocomposites. In the TPU/MCP@ZrP-2% system, the (002) diffraction pattern at 2θ shifted to a lower diffraction angle when compared with TPU/ZrP-2%, resulting in the increase in interlayer space.

The intercalated MCP supramolecules into the interlayer space of α-ZrP sheets promoted further exfoliation, as evidenced by combined TEM images and XRD patterns. The dispersion state of α-ZrP sheets and MCP@ZrP nanohybrids within TPU matrices made the significant difference, which was deemed a critical factor in affecting mechanical property and flame retardancy of TPU nanocomposites.

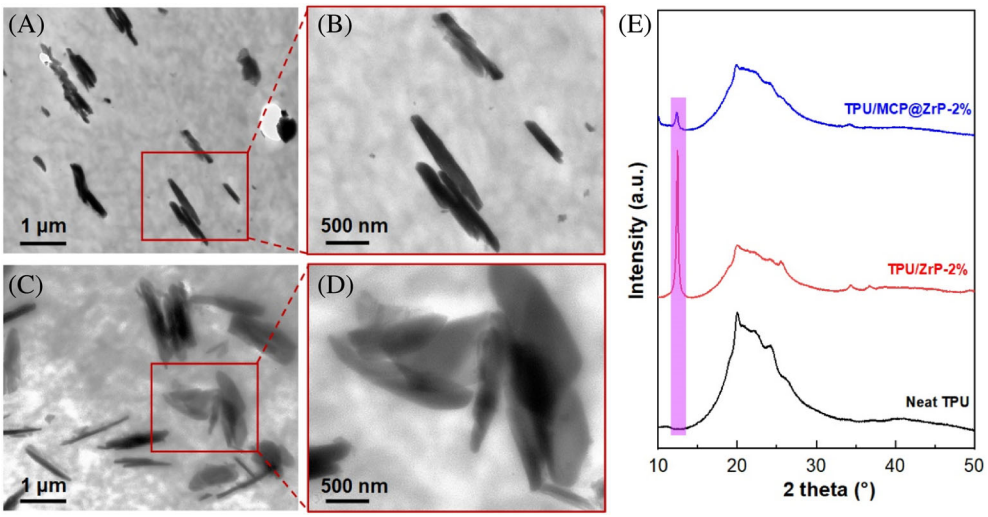

FIGURE 4 Transmission electron microscopy images for (A, B) TPU/ZrP-2% and (C, D) TPU/MCP@ZrP-2%, as well as (E) x-ray diffraction pattern of thermoplastic polyurethane (TPU) and its corresponding nanocomposites.

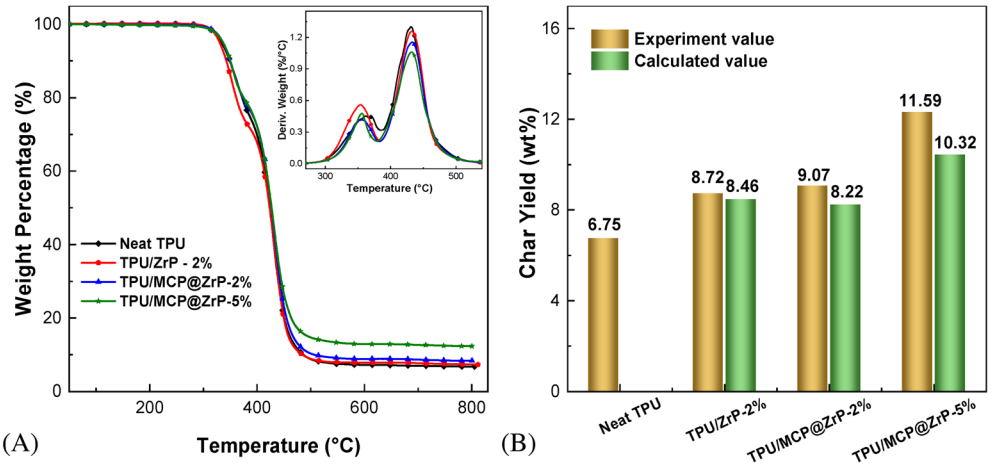

FIGURE 5 (A) Thermal gravimetric analysis thermograms and (B) data comparison between experimental data and calculated results for char yields of thermoplastic polyurethane (TPU) and its nanocomposites under N_2 atmosphere.

3.3 | Thermal stability

Thermal stability of TPU and its nanocomposites was initially investigated using TGA under argon atmosphere prior to the assessment of their flammability. The T_{onset} and the T_{max} were determined at the mass loss of 5 wt% and the peak of DTG curve respectively. The thermal degradation results including T_{onset} and T_{max} were summarized in Table S2.

Under N_2 atmosphere, all TPU samples underwent a two-stage decomposition process in Figure 5A. In the first stage, the degradation of the hard segments takes place due to the relatively lower thermal stability of the urethane groups. The second stage is attributed to the decomposition of the soft segments. To assess the impact of nanofillers on the thermal degradation behavior of TPU, the char yields (CY^{cal}) of TPU and its nanocomposites were determined as follows:

$$CY^{cal} = CY_{TPU} \times f_{w,TPU} + CY_{filler} \times f_{w,filler}, \quad (1)$$

where CY_{TPU} and CY_{filler} denote the residual char yields of TPU and fillers, respectively. Meanwhile, $f_{w,TPU}$ and $f_{w,filler}$ represent the weight fractions of TPU and fillers in the composites. CY^{cal} values of TPU and its nanocomposites were determined from the TGA characterization under N_2 atmosphere according to Figure 5B. It was worth noting that calculated char yields of TPU nanocomposites were lower than those of experimental results. In a typical case, TPU/MCP@ZrP-5% showed an experimental CY value of 11.59%, which was higher than calculated value of 10.32%. Based on the results obtained, synergistic effects between MCP and α-ZrP became evident, which led to the improvement of TPU char residues.

Experimental char yields of TPU/MCP@ZrP nanocomposites were found to be higher than corresponding theoretical values, which indicated the catalytic carbonization function of MCP@ZrP nanohybrids. Furthermore, DTG curves clearly demonstrated that the incorporation of MCP@ZrP nanohybrids significantly reduced the mass loss rate of TPU, which revealed the barrier effect of MCP@ZrP nanohybrid flakes with in-plane oriented direction during thermal degradation.

3.4 | Combustion performance

Cone calorimeter was carried out to evaluate the flame retardancy of α-ZrP and MCP@ZrP nanohybrids in TPU. Several critical parameters determined from the cone calorimeter tests were summarized in Table S3. Figure 6 illustrated the heat release rate (HRR), THR, TSP, and total CO production (TCOP) curves in terms of burning time for TPU nanocomposites. Neat TPU has an intrinsic inflammability with PHRR of 792.45 kW/m^2, THR of 78.81 MJ/m^2 and TSP of 6.38 m^2. The high combustion parameters for neat TPU meant that both heat and smoke hazards could exist in a real fire. The evident suppression on the production of heat and smoke took place with the incorporation of nanoadditives. By adding 5 wt% MCP@ZrP, PHRR, and THR values of nanocomposites were decreased by 35.66% and 18.01% accordingly, resulting in good flame-retardant effectiveness.

MCP supermolecules play a crucial role in facilitating carbonaceous and phosphorus formations at initial stages. Subsequently, the nanobarrier of α-ZrP sheets was beneficial to effectively contain decomposition products at the condensed phase, further promoting the creation of a protective carbon layer. Such a carbon layer was believed to shield underlying polymer matrices from the combustion with the diffusion restriction of degradation products, thereby leading to the obstruction of heat release. In real fire accidents, the accumulation of CO poses a significant

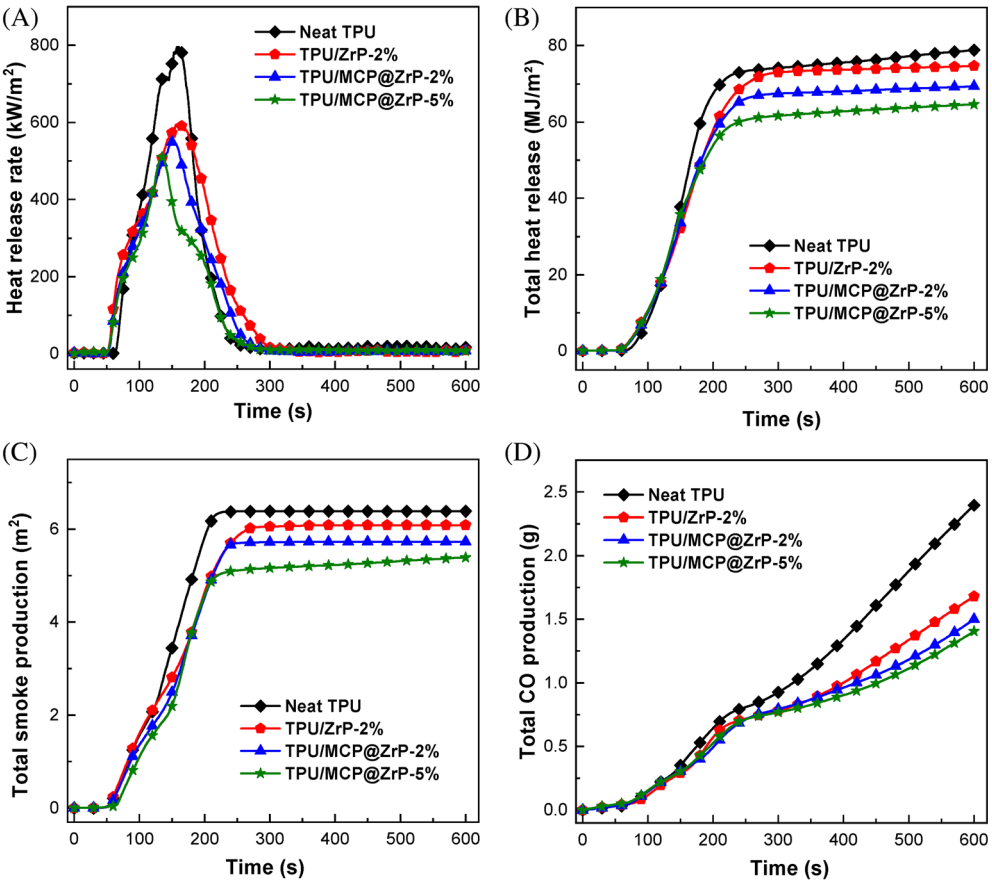

FIGURE 6 (A) Heat release rate, (B) total heat release, (C) total smoke production, and (D) total CO production of neat thermoplastic polyurethane (TPU) and its nanocomposites.

threat, which reflects a more critical role of protective carbon layer. MCP@ZrP nanohybrids yielded a greater reduction in TSP of 15.52% and TCOP when compared with individual α-ZrP sheets. In particular, TPU/MCP@ZrP-5% yielded the lowest TSP and TCOP values, which were reduced by 15.52% and 41.42%, respectively. This phenomenon confirmed excellent suppression effect of smoke and toxic gasses.

Average effective heat of combustion (Av-EHC) serves as an indicator for evaluating the degree of gas phase combustion, and can be used to analyze the gas phase flame-retardant mechanism of MCP@ZrP. As demonstrated in Table S3, the incorporation of MCP@ZrP nanohybrids led to a significant reduction in Av-EHC, along with a lower tendency for the materials to ignite and burn. For instance, Av-EHC of TPU/MCP@ZrP-5% decreased to 18.41 MJ/kg, which was equivalent to approximately 24.46% reduction when compared with that of neat TPU at 24.37 MJ/kg. In the combustion process, MCP degradation creates phosphorous-containing radicals that scavenge active radicals, which effectively terminates the burning chain reaction.[27,28] This enhancement contributed to improving flame retardancy, as well as heat and smoke suppression properties.[29–31]

TABLE 1 Data summary for limiting oxygen index (LOI) and UL-94 tests of thermoplastic polyurethane (TPU) and its nanocomposites.

Sample no.	LOI (vol%)	UL-94 (rating)
Neat TPU	20.5 ± 0.3	No rating
TPU/ZrP-2%	21.6 ± 0.4	No rating
TPU/MCP@ZrP-2%	22.9 ± 0.4	No rating
TPU/MCP@ZrP-5%	24.1 ± 0.5	V-2

The combustion performance of TPU samples was also evaluated by limiting oxygen index (LOI) and vertical burning tests with corresponding data being recorded in Table 1. Neat TPU was flammable with a low LOI value of 20.5%, and thus failed to pass UL-94 vertical tests. In comparison, TPU nanocomposites achieved better performance in LOI and vertical burning tests. After the incorporation of such nanoadditives, LOI values appeared to be increased accordingly. With the same loading of 2 wt% for α-ZrP and MCP@ZrP, LOI values of 21.6% and 22.9% were determined, resulting in better flame-resistant effects with respect to MCP@ZrP. Increasing the addition of MCP@ZrP up to 5 wt% gave rise to a high LOI value of 24.1% by passing the V-2 rating.

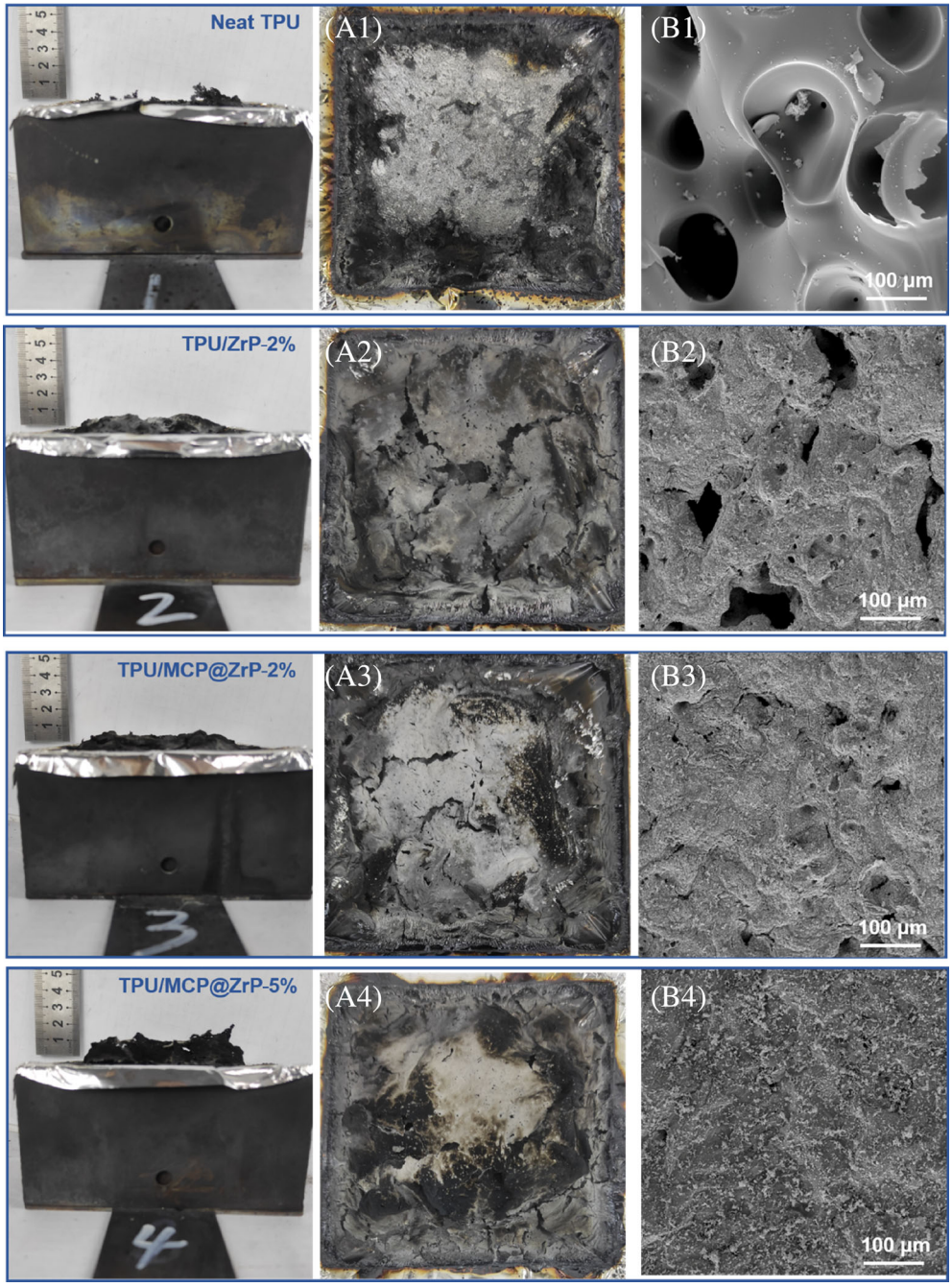

FIGURE 7 (A) Digital photos and (B) scanning electron microscopy images of char residues in thermoplastic polyurethane (TPU) and its nanocomposites.

During LOI and UL-94 tests under small flame, an extinction behavior of polymers could be mainly affected by various aspects, including the decrease in melt viscosity, the improvement in dripping properties, and a decrease in the emission of incombustible gasses. In comparison, the barrier effect of tough inorganic fillers and the formation of char layers became less effective in the improvement of extinguishment effect. Consequently, the improvement in LOI values and UL-94 ratings might be minimal even after the incorporation of flame-retardant additives or fillers. This is because these effects are not primary mechanisms to driving the extinguishment in small-scale flame tests.

3.5 | Analysis of char residues

The morphology and microstructures of residual chars were presented in Figure 7 for the analysis of condensed phase. Apparently, TPU nanocomposites yielded significantly increased residues, which suggested that α-ZrP or MCP@ZrP enabled to promote the carbonization of TPU matrices during the combustion.

The char residues of neat TPU appeared to be loose and broken with plenty of cracks and holes. Whereas, the char residues of TPU nanocomposites became thicker and more compacted with the inclusion of α-ZrP or MCP@ZrP.

The residue chars of neat TPU gave rise to numerous cracks and cavities, making it ineffective in preventing the transfer of toxic and flammable gasses along with the low density of residual char layers. Nonetheless, the addition of MCP@ZrP nanohybrids resulted in less scattered and denser char residues despite the presence of some cracks and cavities. This is because MCP@ZrP nanohybrids have been involved with the carbonization process of TPU, increasing both the quantity and quality of residual chars. In particular, TPU/MCP@ZrP-5% formed a double dense barrier and a more compact carbon layer when compared with neat TPU, as illustrated in Figure 7B. These observations demonstrated that the incorporation of MCP@ZrP nanohybrids into TPU matrices promoted the formation of a dense and robust char layer.

The graphitization degree of char residues was determined using Raman spectra, as depicted in Figure 8. The spectra displayed two distinct peaks centered at approximately 1350 and 1580 cm^{-1}, corresponding to D and G bands, respectively. The area ratio (A_D/A_G) obtained from fitting these peaks indicated the degree of graphitization. The lower A_D/A_G value signifies a higher degree of graphitization. Specifically, the A_D/A_G values for neat TPU, TPU/ZrP-2%, TPU/MCP@ZrP-2%, and TPU/MCP@ZrP-5% were determined to be 2.39, 2.29, 1.61, and 1.45, respectively. It was indicated that the addition of MCP@ZrP nanohybrids enabled to enhance the formation of graphitized char residues with typical shielding effect. This effect enables more effective inhibition of the combustion of the underlying polymer by impeding the transfer of both heat and volatile gasses.

Figure 9A illustrates XRD patterns of char residues. In the case of neat TPU, a prominent and broad peak observed at 24.9° was assigned to (002) lattice planes of graphite, indicating the formation of graphitized carbon. Additionally, two weak peaks were observed at 2θ angles of 19.9° and 33.8° in TPU nanocomposites, corresponding to the lattice planes of α-ZrP. The addition of α-ZrP or MCP@ZrP resulted in a narrower width of the characteristic peak taking place at 24.9° with a clear sign of the increase in near-graphitization. As a result, the presence of MCP@ZrP nanohybrids was believed to effectively enhance the degree of residue graphitization.

The chemical structures of neat TPU and its nanocomposites were determined using FTIR analysis after the combustion. FTIR spectra revealed the presence of C═O and C—O bonds in char residues of neat TPU at 1630 and 1200 cm^{-1}, respectively. In contrast, the intensities of C═O and C—O bonds in FTIR spectra of TPU nanocomposites appeared to be significantly

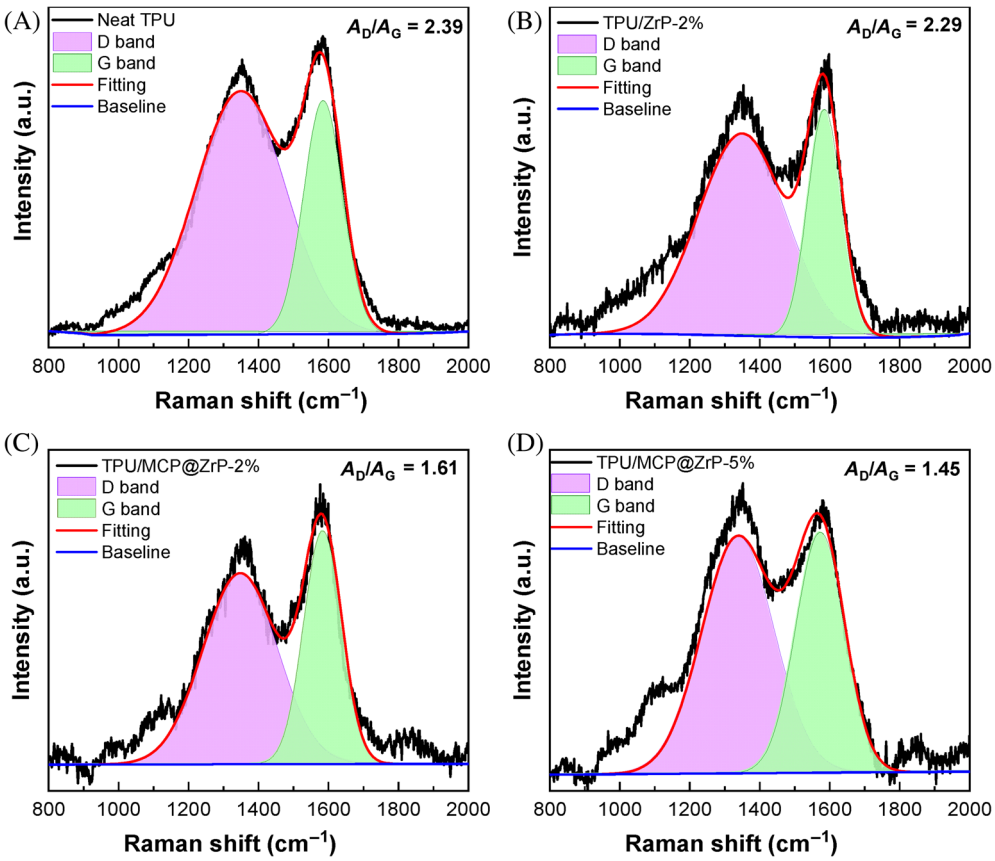

FIGURE 8 Raman spectra of thermoplastic polyurethane (TPU) and its nanocomposites: (A) neat TPU, (B) TPU/ZrP-2%, (C) TPU/MCP@ZrP-2%, and (D) TPU/MCP@ZrP-5%.

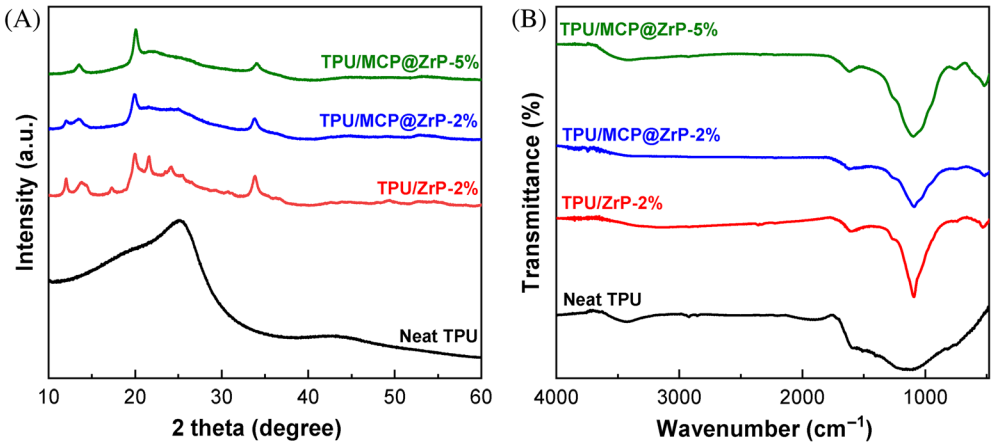

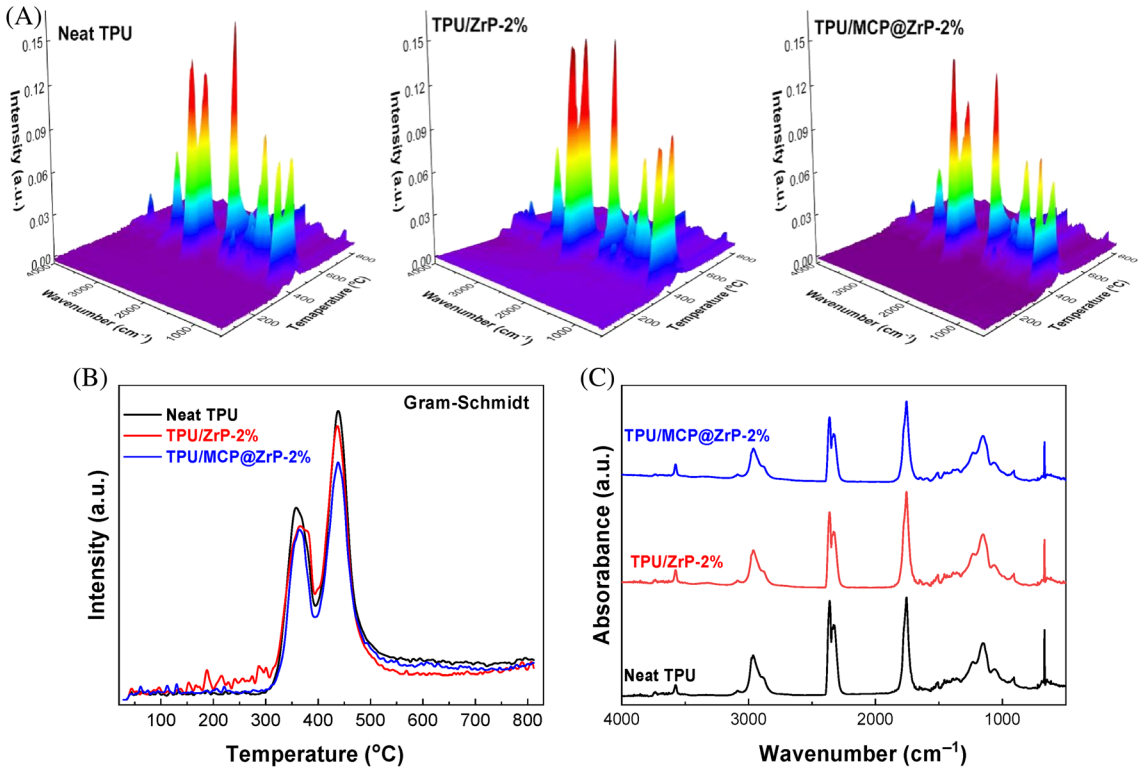

FIGURE 9 (A) X-ray diffraction patterns and (B) Fourier transform infrared spectra of char residues for thermoplastic polyurethane (TPU) and its nanocomposites.

FIGURE 10 TG-FTIR analysis of thermoplastic polyurethane (TPU) and its nanocomposites: (A) 3D data, (B) total pyrolysis products, and (C) FTIR spectra at the maximum decomposition rate. FTIR, Fourier transform infrared; TGA, thermal gravimetric analysis.

lower resulting in a higher degree of graphitization. As for TPU/MCP@ZrP nanocomposites, their FTIR spectra exhibited the characteristic peaks resulting from C—N and C═C bonds at 1403 and 1610 cm^{-1}, respectively. Moreover, two new peaks at 1158 and 1077 cm^{-1} were also observed, corresponding to P—O and P—N—C bending vibrations. The presence of prominent peaks in the XRD patterns of the burned samples containing MCP@ZrP indicated the formation of crosslinked phosphorus oxynitride within the TPU residues.

3.6 | Toxic gas suppression

Figure 10 illustrates the comprehensive analysis of TG-FTIR results conducted to simulate and monitor the release of volatile products during the thermal decomposition process of both neat TPU and its nanocomposites. Figure 10A,B displays 3D FTIR spectra of decomposition products and total pyrolysis products accordingly. Relevant TG-FTIR results in Figure 10 demonstrated that TPU/MCP@ZrP-2% possessed a lower intensity when

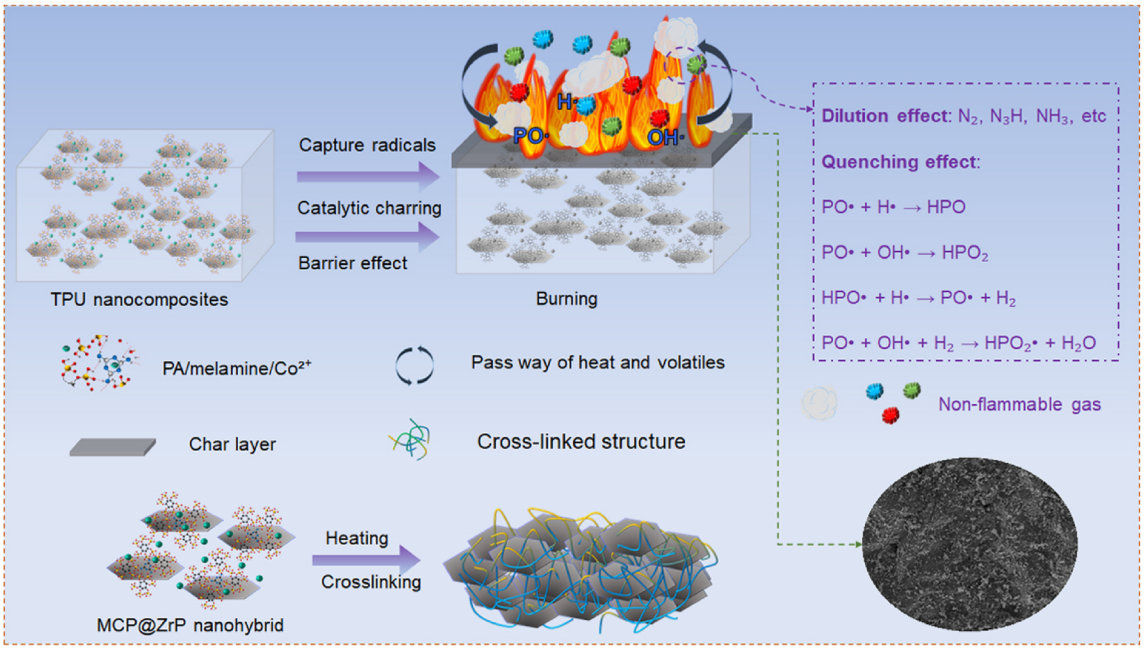

FIGURE 11 Schematic diagram of flame retardant mechanism for MCP@ZrP within thermoplastic polyurethane (TPU) matrices.

compared with neat TPU and TPU/ZrP-2%. It was manifested that the presence of MCP@ZrP nanohybrids resulted in fewer pyrolysis products being released during the thermal decomposition process. Figure 10C revealed characteristic absorption peaks of pyrolysis products at the maximum decomposition rate for neat TPU, TPU/ZrP, and TPU/MCP@ZrP. Such spectra revealed that pyrolysis products of TPU remained similar with composites containing MCP@ZrP nanohybrids. It was inferred that the addition of MCP@ZrP nanohybrids could not alter pyrolysis products of TPU, but rather affected their quantities.

3.7 | Flame retardant mechanism

Based on the combustion behavior analysis carried out, a plausible flame-retardant mechanism of MCP@ZrP nanohybrids was proposed in Figure 11. In the burning process, MCP supermolecules were decomposed and further produced phosphate esters and polyhydric alcohols, thus releasing gaseous NH_3 and H_2O. Simultaneously, TPU chains were decomposed to create polyols and isocyanates. The decomposition of TPU chains resulted in the generation of hydroxyl compounds, which subsequently underwent an esterification reaction with phosphate esters. This reaction led to the formation of a crosslinked network containing aromatic rings.[24]

At elevated temperatures, crosslinked structures were rearranged and further formed more stable carbonous char layers. Moreover, α-ZrP exhibits solid acid catalytic properties, enabling it to facilitate the degradation of TPU chains.[18] TPU decomposition generated long-chain molecules, enabling their absorption onto acidic sites of MCP@ZrP nanohybrids. These adsorbed molecules were further decomposed into smaller carbon chains, which were then catalyzed into residual carbon using sustained heating. This process contributes to the enhanced formation of a continuous and dense residual char layer, which in turn provides superior protection against combustion.[32]

Alongside the aforementioned advantages, MCP@ZrP nanohybrids exhibit high specific surface areas and exceptional thermostability, rendering them ideal insulators for impeding further pyrolysis of TPU chains. During the pyrolysis process of TPU matrices, the presence of α-ZrP promotes physical barrier effect by forming residues with a "labyrinth effect." This effect enhances the compactness and strength of the residues, preventing their agglomeration and ensuring non-agglomerated, randomly distributed arrangement within the matrices.

3.8 | Mechanical and anticorrosion performance

Figure 12 displayed the results of tensile tests carried out on TPU and its nanocomposites in order to evaluate the effect of flame retardants on mechanical performance of TPU nanocomposites. As expected for an elastomer, neat TPU has a low tensile strength with a high elongation at break. However, the addition of nanoadditives significantly increased the breaking strength of TPU nanocomposites

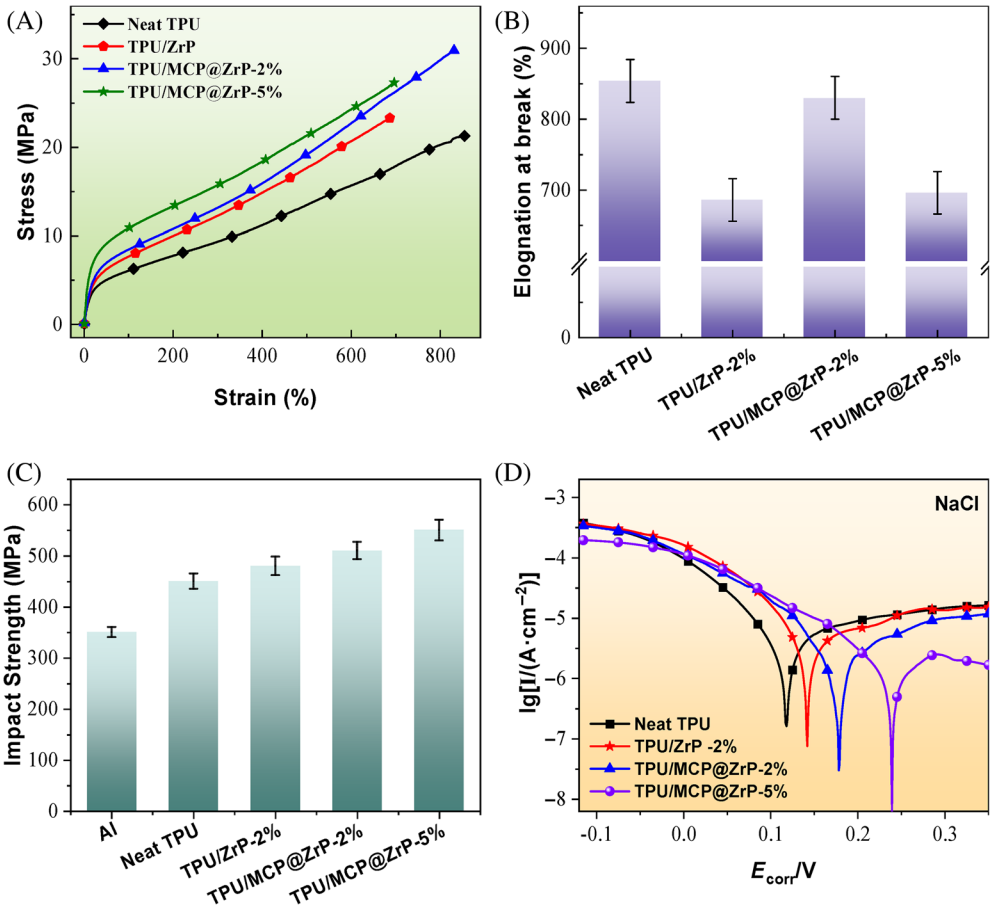

FIGURE 12 (A) Stress–strain curves, (B) elongation at break, (C) impact strength of aluminum alloy and its laminates, and (D) polarization curves of thermoplastic polyurethane (TPU) and its nanocomposites.

over that of neat TPU. The incorporation of MCP@ZrP nanohybrids led to the formation of hydrogen interactions between MCP@ZrP and TPU chains, resulting in strong interfacial interactions with TPU matrices. Such interactions enhanced the mechanical performance of TPU nanocomposites accordingly. As such, with the same addition of 2 wt%, the tensile strength of TPU/MCP@ZrP reached 30.94 MPa, which was superior to that of TPU/ZrP at 23.31 MPa. The significant improvement in mechanical performance, observed in TPU nanocomposites due to the addition of MCP@ZrP nanohybrids, would offer great advantages for their widespread use in engineering fields. These enhanced mechanical behaviors can lead to improved durability and reliability, as well as higher load-bearing capacity and resistance to impact and deformation loads. Overall, the incorporation of MCP@ZrP nanohybrids as flame retardants into TPU matrices shows great potential to the development of advanced engineering materials with superior mechanical performance.

Figure 12C illustrates the impact resistance of 6061 aluminum alloy and its laminates coated with TPU nanocomposites. The impact strength of the alloy was measured to be 349 ± 10 kJ/m^2. Introducing 2-mm thick neat TPU films on one surface of the alloy sheet resulted in an increased impact strength of 450 ± 15 kJ/m^2, representing a notable increment of 28.94%. However, when TPU nanocomposites were used, even greater increments were observed. Overall, the laminates containing TPU nanocomposites exhibited significantly higher impact resistance compared with that of neat TPU system. Among the TPU/MCP@ZrP systems, those with a composition of 5 wt % demonstrated the highest impact strength values, reaching 550 ± 17 kJ/m^2, which is an exceptional improvement of 57.59% compared with the uncoated alloy sheet.

The composite films hybrided with 2 D nanosheets will present good barrier property by forming a tortuous path for the gas/liquid to travel. Therefore, it is of great potential for TPU film used in anticorrosive environment. The polarization curves of TPU and its nanocomposite films immersed in 3.5 wt% NaCl solution are shown in Figure 12D. The electrochemical parameters, such as corrosion potential (E_{corr}) and corrosion current density (I_{corr}), were analyzed using electrochemical software through Tafel extrapolation.[33] This analysis provided valuable insights into the corrosion behavior of the material. TPU/ZrP-2%, TPU/MCP@ZrP-2%, and TPU/MCP@ZrP-5% have E_{corr} of 0.142, 0.178, and 0.239 V, which are significantly better than neat TPU (0.117 V). As for I_{corr}, ZrP incorporated TPU composites show a decreased corrosion current density with respect to pure TPU, indicative of the

barrier effect of ZrP nanosheets on the corrosion liquid. At the same time, TPU/MCP@ZrP-2% (0.79×10^{-6}A/cm^2) shows a lower corrosion current density than TPU/ZrP-2% (1.58×10^{-6}A/cm^2). I_{corr} of TPU/MCP@ZrP-5% (5.01×10^{-7}A/cm^2) is one magnitude of order lower I_{corr} than that of neat TPU (3.16×10^{-6}A/cm^2). The higher E_{corr} and lower I_{corr} of TPU/MCP@ZrP-5% film indicate its better corrosive resistance with respect to other films. Therefore, TPU/MCP@ZrP film shows improved anticorrosive property and flame retardancy, which is promising in harsh environment.

4 | CONCLUSIONS

In this study, novel MCP@ZrP nanohybrids were prepared via melamine/Co^{2+}/phytic-acid self-assembled on α-ZrP nanosheet surfaces. MCP@ZrP nanohybrids were detected to enhance mechanical properties, thermal stability, flame retardancy, and smoke suppression of TPU nanocomposites. The morphology and microstructural analysis revealed that the compatibility and dispersion state of α-ZrP nanosheets within TPU matrices were improved via wrapping MCP supermolecules onto α-ZrP nanosheets. The addition of 5.0 wt% MCP@ZrP to TPU nanocomposites resulted in remarkable reductions of 35.66% and 18.01% in PHRR and THR, respectively. Catalytic charring and physical barrier effect of nanohybrids formed more integrated and compact char layers in order to enhance fire safety and smoke suppression of TPU nanocomposites. This study not only tackles great challenges to dispersing and compatibilizing α-ZrP sheets but also offers a practical solution to enhancing the flame retardancy of TPU. Significant implications from this study benefit various industrial applications where it is essential to develop high-performance materials with superior resistance to impact and corrosion, and excellent fire safety.

ACKNOWLEDGMENTS

The first author would like to acknowledge Shiyanjia Lab (www.shiyanjia.com) for the technical support in SEM analysis. This work was financially supported by the National Natural Science Foundation of China (52173077), the Liaoning Provincial Department of Education Series Project, China (LJKZ0187), the Natural Science Foundation of Liaoning Province (2023-MS-239), and the Liaoning BaiQianWan Talents Program, China (2021921081). Open access publishing facilitated by Curtin University, as part of the Wiley - Curtin University agreement via the Council of Australian University Librarians.

DATA AVAILABILITY STATEMENT

Data will be made available on request.

ORCID

Yu Dong https://orcid.org/0000-0003-1774-1553

REFERENCES

1. Xue R, He S, He Y, et al. Enhanced dielectric, energy storage, and actuated performance of TPU/BaTiO3 dielectric elastomer composites by thermal treatment. *Polym Compos*. 2023;44(2):992-1003. doi:10.1002/pc.27149
2. Zou H, Ran Q, Wu S, Shen J. Study of nanocomposites prepared by melt blending TPU and montmorillonite. *Polym Compos*. 2008;29(4):385-389. doi:10.1002/pc.20406
3. Tayfun U, Dogan M, Bayramli E. Effect of surface modification of rice straw on mechanical and flow properties of TPU-based green composites. *Polym Compos*. 2016;37(5):1596-1602. doi:10.1002/pc.23331
4. Li J, Wu W, Hu H, Rui Z, Zhao T, Zhang X. The synergism effect of montmorillonite on the intumescent flame retardant thermoplastic polyurethane composites prepared by selective laser sintering. *Polym Compos*. 2022;43(9):5863-5876. doi:10.1002/pc.26621
5. Wang X-C, Geng T, Han J, et al. Effects of nanoclays on the thermal stability and flame retardancy of microcellular thermoplastic polyurethane nanocomposites. *Polym Compos*. 2018;39(S3):E1429-E1440. doi:10.1002/pc.24340
6. Tai Q, Shan X, Song L, Lo S, Yuen RKK, Hu Y. A polymeric flame retardant and surfactant-free montmorillonite nanocomposites: preparation and exfoliation mechanism discussion. *Polym Compos*. 2014;35(1):167-173. doi:10.1002/pc.22646
7. Liu B-W, Zhao H-B, Wang Y-Z. Advanced flame-retardant methods for polymeric materials. *Adv Mater*. 2022;34(46):2107905. doi:10.1002/adma.202107905
8. Lin X-C, Li S-L, Li W-X, et al. Thermo-responsive self-ceramifiable robust aerogel with exceptional strengthening and thermal insulating performance at ultrahigh temperatures. *Adv Funct Mater*. 2023;33(27):2214913. doi:10.1002/adfm.202214913
9. Wang ZH, Liu BW, Zeng FR, et al. Fully recyclable multifunctional adhesive with high durability, transparency, flame retardancy, and harsh-environment resistance. *Sci Adv*. 2022;8(50):eadd8527. doi:10.1126/sciadv.add8527
10. Zhang L, Zheng G-Q, Chen X-L, et al. Smart self-puffing phosphite-protonated siloxane network enables multifunctional transparent protection. *ACS Mater Lett*. 2023;5(9):2398-2407. doi:10.1021/acsmaterialslett.3c00755
11. Shi Y, Liu C, Duan Z, Yu B, Liu M, Song P. Interface engineering of MXene towards super-tough and strong polymer nanocomposites with high ductility and excellent fire safety. *Chem Eng J*. 2020;399:125829. doi:10.1016/j.cej.2020.125829
12. Wang J, Zhang D, Zhang Y, et al. Construction of multifunctional boron nitride nanosheet towards reducing toxic volatiles (CO and HCN) generation and fire hazard of thermoplastic polyurethane. *J Hazard Mater*. 2019;362:482-494. doi:10.1016/j.jhazmat.2018.09.009
13. Cai W, Wang B, Liu L, et al. An operable platform towards functionalization of chemically inert boron nitride nanosheets for flame retardancy and toxic gas suppression of thermoplastic polyurethane. *Compos B Eng*. 2019;178:107462. doi:10.1016/j.compositesb.2019.107462
14. Cai W, Li Z, Mu X, et al. Barrier function of graphene for suppressing the smoke toxicity of polymer/black phosphorous

nanocomposites with mechanism change. *J Hazard Mater*. 2021;404(Pt A):124106. doi:10.1016/j.jhazmat.2020.124106

15. Wu W, Zhao W, Gong X, et al. Surface decoration of Halloysite nanotubes with POSS for fire-safe thermoplastic polyurethane nanocomposites. *J Mater Sci Technol*. 2022;101:107-117. doi:10.1016/j.jmst.2021.05.060
16. Han S, Yang F, Meng Q, et al. Using renewable phosphate to decorate graphene nanoplatelets for flame-retarding, mechanically resilient epoxy nanocomposites. *Prog Org Coat*. 2023;182:107658. doi:10.1016/j.porgcoat.2023.107658
17. Han S, Yang F, Li Q, et al. Tackling smoke toxicity and fire hazards of thermoplastic polyurethane by mechanochemical combination of Cu_2O nanoparticles and zirconium phosphate nanosheets. *Polym Degrad Stab*. 2023;212:110350. doi:10.1016/j.polymdegradstab.2023.110350
18. Han S, Yang F, Li Q, Sui G, Kalimuldina G, Araby S. Synergetic effect of alpha-ZrP nanosheets and nitrogen-based flame retardants on thermoplastic polyurethane. *ACS Appl Mater Interfaces*. 2023;15(13):17054-17069. doi:10.1021/acsami.2c20482
19. Han S, Li Q, Ma N, Liu D, Sui G, Araby S. Supramolecular-wrapped α-zirconium phosphate nanohybrid for fire safety and reduced toxic emissions of thermoplastic polyurethane. *ACS Appl Polym Mater*. 2024;6:1376-1388. doi:10.1021/acsapm.3c02481
20. Ren J, Wang Y, Piao J, et al. Facile construction of organic–inorganic hybrid flame-retardant system based on fully biomass: improving the fire safety and mechanical property of epoxy resin. *Chem Eng J*. 2023;460:141775. doi:10.1016/j.cej.2023.141775
21. Ren J, Huo S, Huang G, et al. A novel P/Ni-doped g-C3N4 nanosheets for improving mechanical, thermal and flame-retardant properties of acrylonitrile–butadienestyrene resin. *Chem Eng J*. 2023;452:139196. doi:10.1016/j.cej.2022.139196
22. Qu Z, Wu K, Jiao E, et al. Surface functionalization of few-layer black phosphorene and its flame retardancy in epoxy resin. *Chem Eng J*. 2020;382:122991. doi:10.1016/j.cej.2019.122991
23. Jiang H, Xie Y, Zhu R, et al. Construction of polyphosphazene-functionalized $Ti_3C_2T_X$ with high efficient flame retardancy for epoxy and its synergetic mechanisms. *Chem Eng J*. 2023;456:141049. doi:10.1016/j.cej.2022.141049
24. Luo Y, Xie Y, Geng W, et al. Fabrication of thermoplastic polyurethane with functionalized MXene towards high mechanical strength, flame-retardant, and smoke suppression properties. *J Colloid Interface Sci*. 2022;606(Pt 1):223-235. doi:10.1016/j.jcis.2021.08.025
25. Qiu S, Hou Y, Xing W, et al. Self-assembled supermolecular aggregate supported on boron nitride nanoplatelets for flame retardant and friction application. *Chem Eng J*. 2018;349:223-234. doi:10.1016/j.cej.2018.05.053
26. Cai W, Hong N, Feng X, et al. A facile strategy to simultaneously exfoliate and functionalize boron nitride nanosheets via Lewis acid-base interaction. *Chem Eng J*. 2017;330:309-321. doi:10.1016/j.cej.2017.07.162
27. Huang G, Han D, Jin Y, Song P, Yan Q, Gao C. Fabrication of nitrogen-doped graphene decorated with organophosphor and lanthanum toward high-performance ABS nanocomposites. *ACS Appl Nano Mater*. 2018;1(7):3204-3213. doi:10.1021/acsanm.8b00411
28. Fang F, Ran S, Fang Z, Song P, Wang H. Improved flame resistance and thermo-mechanical properties of epoxy resin nanocomposites from functionalized graphene oxide via self-assembly in water. *Compos B Eng*. 2019;165:406-416. doi:10.1016/j.compositesb.2019.01.086
29. Wang Y, Zhang Y, Ma L, et al. Facile synthesis of phosphorus-containing benzotriazole flame retardant for enhancement of mechanical and fire properties of epoxy resins. *Eur Polym J*. 2024;202:112610. doi:10.1016/j.eurpolymj.2023.112610
30. Wang Y, Ma L, Wang H, Cheng C, Yin X, Zhu Z. Fabrication of a flame retardant, strong mechanical toughness and antimicrobial polylactic acid by chitosan Schiff base/ammonium polyphosphate. *Polym Degrad Stab*. 2023;216:110492. doi:10.1016/j.polymdegradstab.2023.110492
31. Wang Y, Ma L, Yuan J, et al. A green flame retardant by elaborate designing towards multifunctional fire-safety epoxy resin composites. *React Funct Polym*. 2023;191:105677. doi:10.1016/j.reactfunctpolym.2023.105677
32. He L, Wang J, Wang B, et al. Large-scale production of simultaneously exfoliated and functionalized Mxenes as promising flame retardant for polyurethane. *Compos B Eng*. 2019;179:107486. doi:10.1016/j.compositesb.2019.107486
33. Huang H, Li M, Tian Y, et al. Exfoliation and functionalization of α-zirconium phosphate in one pot for waterborne epoxy coatings with enhanced anticorrosion performance. *Prog Org Coat*. 2020;138:105390. doi:10.1016/j.porgcoat.2019.105390

SUPPORTING INFORMATION

Additional supporting information can be found online in the Supporting Information section at the end of this article.

How to cite this article: Han S, Li S, Liu D, et al. Enhancing flame retardancy, anti-impact, and corrosive resistance of TPU nanocomposites using surface decoration of α-ZrP. *Polym Compos*. 2024; 1-15. doi:10.1002/pc.28404